



LUND UNIVERSITY

Fiber-based stray light suppression in spectroscopy using periodic shadowing

Gong, Miaoxin; Kim, Haisol; Larsson, Jim; Methling, Torsten; Aldén, Marcus; Kristensson, Elias; Brackmann, Christian; Eschrich, Tina; Jäger, Matthias; Kiefer, Wolfgang; Ehn, Andreas

Published in:
Optics Express

DOI:
[10.1364/OE.410517](https://doi.org/10.1364/OE.410517)

2021

Document Version:
Publisher's PDF, also known as Version of record

[Link to publication](#)

Citation for published version (APA):

Gong, M., Kim, H., Larsson, J., Methling, T., Aldén, M., Kristensson, E., Brackmann, C., Eschrich, T., Jäger, M., Kiefer, W., & Ehn, A. (2021). Fiber-based stray light suppression in spectroscopy using periodic shadowing. *Optics Express*, 29(5), 7232-7246. <https://doi.org/10.1364/OE.410517>

Total number of authors:
11

Creative Commons License:
CC BY

General rights

Unless other specific re-use rights are stated the following general rights apply:
Copyright and moral rights for the publications made accessible in the public portal are retained by the authors and/or other copyright owners and it is a condition of accessing publications that users recognise and abide by the legal requirements associated with these rights.

- Users may download and print one copy of any publication from the public portal for the purpose of private study or research.
- You may not further distribute the material or use it for any profit-making activity or commercial gain
- You may freely distribute the URL identifying the publication in the public portal

Read more about Creative commons licenses: <https://creativecommons.org/licenses/>

Take down policy




If you believe that this document breaches copyright please contact us providing details, and we will remove access to the work immediately and investigate your claim.

LUND UNIVERSITY

PO Box 117
221 00 Lund
+46 46-222 00 00



Fiber-based stray light suppression in spectroscopy using periodic shadowing

MIAOXIN GONG,¹ HAISOL KIM,¹  JIM LARSSON,¹ TORSTEN METHLING,¹ MARCUS ALDÉN,¹  ELIAS KRISTENSSON,¹ CHRISTIAN BRACKMANN,¹  TINA ESCHRICH,² MATTHIAS JÄGER,² WOLFGANG KIEFER,^{3,4} AND ANDREAS EHN^{1,*}

¹Division of Combustion Physics, Lund University, Box 118, Lund SE-22100, Sweden

²Leibniz Institute of Photonic Technology, Albert Einstein St. 9, 07745 Jena, Germany

³Institute for Physical and Theoretical Chemistry, University of Würzburg, 97074 Würzburg, Germany

⁴Eisingen Laboratory for Applied Raman Spectroscopy, 97249 Eisingen, Germany

*andreas.ehn@forbrf.lth.se

Abstract: Stray light is a known strong interference in spectroscopic measurements. Photons from high-intensity signals that are scattered inside the spectrometer, or photons that enter the detector through unintended ways, will be added to the spectrum as an interference signal. A general experimental solution to this problem is presented here by introducing a customized fiber for signal collection. The fiber-mount to the spectrometer consists of a periodically arranged fiber array that, combined with lock-in analysis of the data, is capable of suppressing stray light for improved spectroscopy. The method, which is referred to as fiber-based periodic shadowing, was applied to Raman spectroscopy in combustion. The fiber-based stray-light suppression method is implemented in an experimental setup with a high-power high-repetition-rate laser system used for Raman measurements in different room-temperature gas mixtures and a premixed flame. It is shown that the stray-light level is reduced by up to a factor of 80. Weak spectral lines can be distinguished, and therefore better molecular species identification, as well as concentration and temperature evaluation, were performed. The results show that the method is feasible and efficient in practical use and that it can be employed as a general tool for improving spectroscopic accuracy.

© 2021 Optical Society of America under the terms of the [OSA Open Access Publishing Agreement](#)

1. Introduction

Laser-based spectroscopic methods have a wide range of applications in a number of research fields, including fundamental physics, astronomy [1, 2], biomedicine [3–5], materials science [5], combustion science [6], plasma research [7], etc. Among modern optical instruments, fibers have been employed in a variety of spectroscopic applications with several advantages [8]. Fiber-based sampling systems allow the sample to be analyzed remotely from the optical instrumentation, which is especially useful in investigating hostile environments. The chemically reactive flows in combustion with high temperatures and intense heat transfer, for example, result in harsh experimental conditions. Laser-based spectroscopic methods are beneficial tools to investigate such phenomena in-situ and non-intrusively with high accuracy [9].

Stray light in a spectrometer system can be described as light that deviates from the intended path and distorts the spectral characteristics of the detected light [10–12]. Stray light originates from various sources, for example, surface imperfections of the optical components and particles or droplets in the optical path [13]. Stray light can be a severe problem in spectral analysis of signals, especially when the spectral shift from the laser wavelength is small and the signal of interest is weak. Moreover, stray light presents a general experimental challenge for in-situ diagnostics of processes, e.g., for measurements in reactors and/or in the vicinity of surfaces.

Therefore, it is often necessary to eliminate or correct the signal for stray light in the spectroscopic measurements, especially when quantitative analysis is desired. Optical filters provide the traditional solution to suppress background light in a certain wavelength range, such as the spectral width of a laser line, that enters the spectrometer, see for example [14]. In addition to filters based on conventional optical materials, vapor of strongly absorbing atomic species, such as K, Hg, I, Rb, or Na, have been employed as efficient and spectrally narrow filters [15–21]. Another optical solution is provided by double or triple monochromators for stray light reduction [10, 22–24]. Yet, such a method results in the loss of collected light, detrimental for the detection of low signals, and also prevents multiplex spectroscopic measurements as the monochromator requires scanning for registration of a spectrum. In some cases, computer-assisted stray-light correction approaches are feasible, and a method based on analysis of spectrum derivatives is mostly used [25, 26]. However, the ability to remove stray light using the derivative approach is dependent on that the gradients of the stray-light signal and the signal of interest are different, which generally cannot be assumed.

A general experimental solution to the stray-light problem in spectroscopy, referred to as Periodic Shadowing (PS), was presented by Kristensson et al. [27]. The PS concept is the combination of the analog implementation of a periodic pattern onto the signal before reaching the detector, inspired by Structured Illumination Microscopy [28], and the following data processing based on lock-in analysis [29]. The concept was successfully demonstrated for stray-light suppression in a wide range of spectroscopic techniques based on emission, absorption, scattering, and nonlinear coherent optical processes. The experiments were done with optics arranged for open-space collection of light and a transmission grating mounted on the spectrometer entrance slit. The latter is a fundamental part of the PS concept in order to imprint a periodic pattern on the collected signal, which is necessary for further processing. Since the PS concept in this first version proved to be a highly versatile and powerful method for stray-light suppression, a natural next step is to increase its feasibility, strength, and robustness in spectroscopic applications. In this paper, we, therefore, present a novel fiber-based stray-light suppression method based on the PS concept. The fiber-based PS method is implemented with a custom-made array of optical fibers, which enables flexible signal collection combined with stray-light suppression by means of the PS method. The experimental arrangement employs the PS-fiber to deliver the signal light and create the periodic pattern, which is needed for further data processing. A schematic description of the major issues and their corresponding solutions that are addressed in this work is shown in Fig. 1.

The new method is demonstrated with Raman spectroscopy, based on inelastic scattering of laser photons, which is a commonly employed technique for the detection of chemical species in analyses of solid, liquid, and gaseous samples [30]. However, the inherent weakness of the signals from the inelastic scattering makes Raman spectroscopy in the gas phase challenging. Raman spectroscopy is a linear process where more incident photons enhance the signal, and thus a laser of high average power can be used to compensate for weak signals, but then also increases potential interference from stray light. Raman spectroscopy in studies of combustion processes necessitates the detection of species in a gas-phase environment with high background luminosity. While pulsed lasers and gated detection allow for the rejection of continuous background signals, combustion diagnostics nevertheless represents an experimental challenge for Raman spectroscopy. Great care must be taken to distinguish Raman signals from stray light of the laser source and strong Rayleigh and Mie scattering signals, as well as other types of interfering signal contributions [31,32]. The fiber-based PS method has thus been investigated under such conditions by measurements in gases at ambient conditions and in premixed flames. The method has been characterized for suppression of different stray-light levels, and evaluated O₂ mole fractions and temperatures have been assessed to ensure that accurate quantitative information is retrieved from spectra after processing.

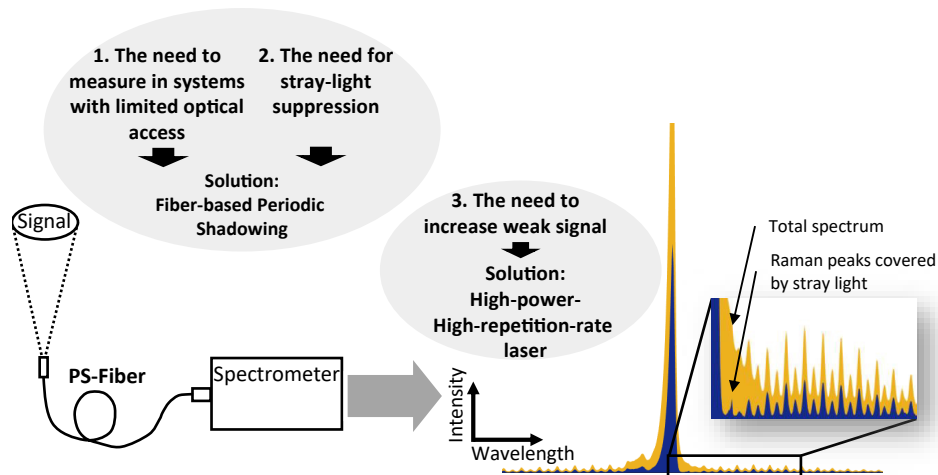


Fig. 1. Schematic diagram illustrating the main challenges and the solutions used in this paper. The experimental arrangement contains the PS-fiber employed to deliver signal light. The spectrum is a typical vibrational Raman spectrum of nitrogen, where the yellow area is the total spectrum, and the blue area is the Raman signal components after rejecting interfering stray light using periodic shadowing.

2. Method

2.1. Fiber based periodic shadowing

The predefined pattern was in the previous study created by a transmissive Ronchi grating placed at the entrance slit of the spectrometer [27], which blocks 50% of the incoming light. Here, as shown in Fig. 2(a), a specialized fiber-optic bundle is used instead. The transmitted light through the Ronchi grating has the modulation of a square wave which is very close to what is achieved with the fiber, as is shown in Fig. 2(b).

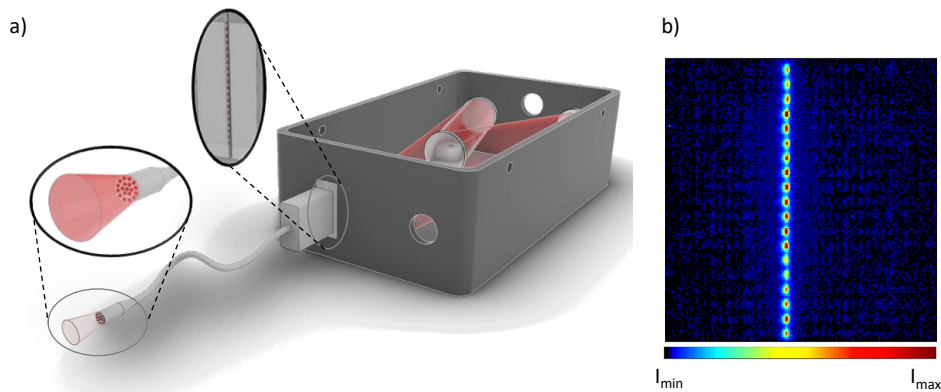


Fig. 2. a) Schematic view of the experimental arrangement. The PS-fiber bundle collects signal light and modulates it into the predefined pattern. b) Unprocessed PS spectrum of vibrational Raman signal of nitrogen at 2331 cm^{-1} in which the predefined pattern of periodic feature can be observed.

The customized silicon fiber manufactured for the PS method is shown in Fig. 3.

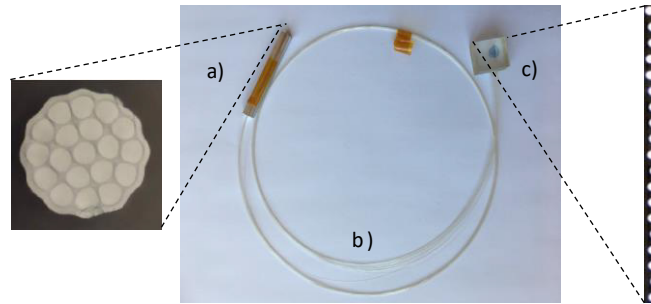


Fig. 3. Illustration and photographs of the custom-made PS fiber. a) and c) show the input end and the output end of the PS fiber with sectional views, respectively. b) shows the extension of the fiber bundle.

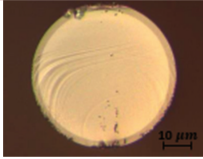
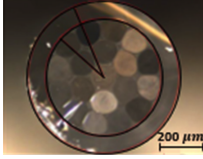
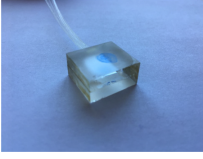
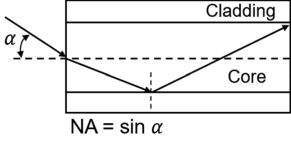
Each PS fiber bundle contains 19 individual and identical multimode fibers, which are arranged into a circular arrangement at the input end and a linear array at the output end. For this purpose, the coatings of the fibers have been stripped on both sides, but the light-guiding in each of the F300 pure silica cores is still provided by the thin fluorine-doped cladding with a numerical aperture of 0.22 (see Table 1 for additional fiber details). The fiber itself has been manufactured at the Leibniz IPHT with the exception of the fluorine-doped cladding (deposited at the Heraeus Comvance company). The round fiber bundle has been inserted into an F300 silica capillary, and the arrangement has been fused together using a Vytran GPX 3200 glass processing machine by applying a vacuum and only gave minor changes in the fiber dimensions. The bundle was finally cleaved to obtain the input facet.

On the output side, the fibers have been arranged in a linear periodic fashion: each active fiber (guidance fiber) is separated by a short piece of identical ‘dead’ fiber (distance fiber) in which no light is transmitted so that a unique pattern with a fixed spatial frequency is created when light is inserted into the input end. The results of such an arrangement, as the fiber is mounted onto the slit, is a periodic pattern that is close to a square wave modulation. Care has been taken to place the central input fiber in the middle of the linear output side. Towards each end of the linear arrangement follow three of the six fibers from the inner input ring and finally the fibers of the outer ring. The individual fibers are bonded using epoxy between two BK7 glass blocks with 130 μm separation. The output facet was obtained by polishing.

The PS fiber transmits the light and forms a predefined spatial modulation pattern at the same time. The introduction of the fiber, in principle, improves the transmission efficiency as it avoids the 50% blockage of light at the slit encountered when using Ronchi gratings. Fiber optics also simplifies the alignment and allows more flexibility in the optical system [8]. In many experiments where optical access is exceedingly limited (e.g., in combustion engines), fiber optics serve as a probe to such environments. The parameters in Table 1 show the dimensions of the optical fibers, which should be related to the spectrometer. The round fiber configuration at the input end assures that the fiber bundle maintains the same numerical aperture (NA) as the individual fibers. In addition, the coupling of the light into the multimode fiber has a considerable effect on its performance. In order to fully utilize the collected signal, the NA of the input light cone has to be less than that of the fiber, i.e., underfilling the fiber.

When the camera registers the light after dispersion, a 2D spectral image is captured that can be further processed in the stray-light removal lock-in algorithm, shown in Fig. 4. Modulated raw input data and the post-processed output data are shown in Fig. 4(i) and 4ii, respectively. The three necessary processing steps, along with a graphical description of the filter function that

Table 1. Important parameters of the PS fiber.

	Approximate dimensions	Photograph
Each individual fiber	Fiber core diameter: 114 μm Cladding diameter: 126 μm Coating diameter: 230 μm	
The input end of the PS fiber bundle	Outer diameter: ~ 1610 μm Inner diameter: ~ 1294 μm	
The output end of the PS fiber bundle	LWH of the glass holder: 2.0 × 1.0 × 0.5 cm	
Numerical Aperture (NA)	0.22 ± 0.02	

is used in the process, is displayed in Fig. 4(a)-(d). The processing of the modulated image is described in detail by Kristensson et al. [27]. In summary, the signal-processing algorithm is carried out by first using fast Fourier transform (FFT) on the modulated spectral image (Fig. 3(i)) column by column, providing a stack of 1D Fourier transforms (Fig. 3(a)). Each column is then multiplied with two reference signals with a 90° relative phase shift, transforming the periodic component into a DC component. This operation will cause the stray light, which originally is a DC component, to shift into higher frequencies, which is shown in the close-up inset in Fig. 3(b). After applying the band-pass filter, shown in Fig. 3(c), the non-modulated stray-light component can be removed, as shown in Fig. 3(d). The final spectrum, with minimal stray light interference, displayed in Fig. 3(ii), is finally obtained by an inverse Fourier transform.

The input data in the periodic shadowing algorithm has to have a periodic modulation, ideally sinusoidal, in order for this demodulation scheme to work. A modulation that deviates from a sinusoidal modulation will have overtone components in its Fourier transform. Such overtones will simply be disregarded in the periodic shadowing processing and will thus not cause any implication for the method except that the signal contribution in these overtones will be lost. These overtones are really small with this fiber arrangement, which is seen in Fig. 4(a) where they are barely visible.

2.2. Raman spectroscopy

An Nd:YAG laser (HD40I-OE, Edgewave, 100 W), operating at 5 kHz with pulses of ~12 ns duration, was used to perform Raman spectroscopy in this investigation. The laser delivered an average power of 25 W, which is 25% of the maximum power, at a wavelength of 532 nm.

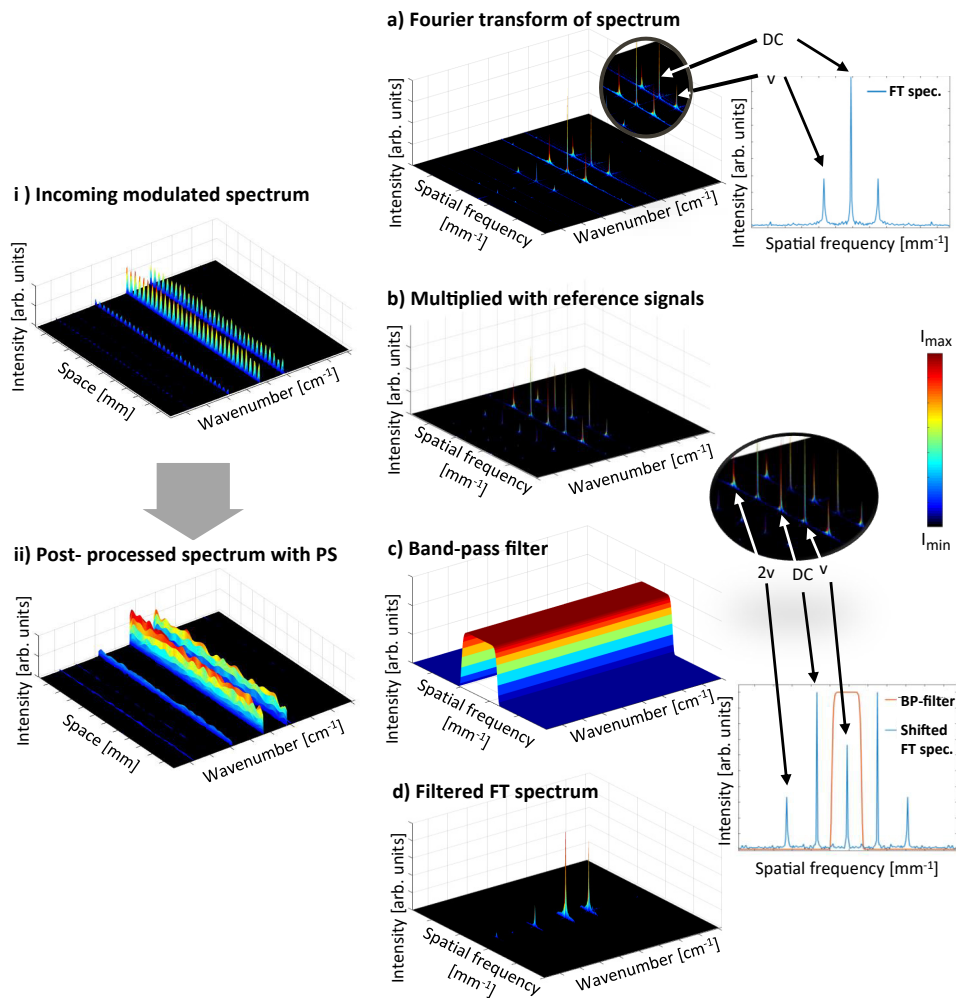


Fig. 4. Data processing of the Periodic shadowing method. i) and ii) illustrate the spectra before and after the PS process, respectively. a)-d). a) Fourier transform of the spectrum; b) multiplication with reference signals to place the fundamental peak at the origin and the DC component to $\pm v$ in the spatial frequency domain; c) application of a band-pass filter to extract the information of the modulation while filtering out components with high spatial frequencies; d) Fourier transformed spectrum after filtering.

A schematic experimental setup is shown in Fig. 5. A multi-pass arrangement, displayed in Ref. [33], was used to increase the laser irradiance in the measurement volume and enhance the Raman signal. The multi-pass optics included a lens (L1) with focal length $f=300$ mm and a cavity with a pair of dichroic multi-pass mirrors (MP) with focal length $f=100$ mm and radius $r=50$ mm. The laser beam was guided into the cavity through a hole on the edge of the first multi-pass mirror and focused at the center of the cavity by the lens. The laser beam was then reflected back and forth between the multi-pass mirrors 32 times, with focal points located at the center of the cavity. This resulted in a probe volume with dimensions of approximately $5 \times 2 \times 1$ mm³.

The Raman scattering signal was collected by a set of two achromatic lenses (L2 and L3) with a focal length of 200 mm each. In addition, a concave aluminum mirror (M4) with a focal length

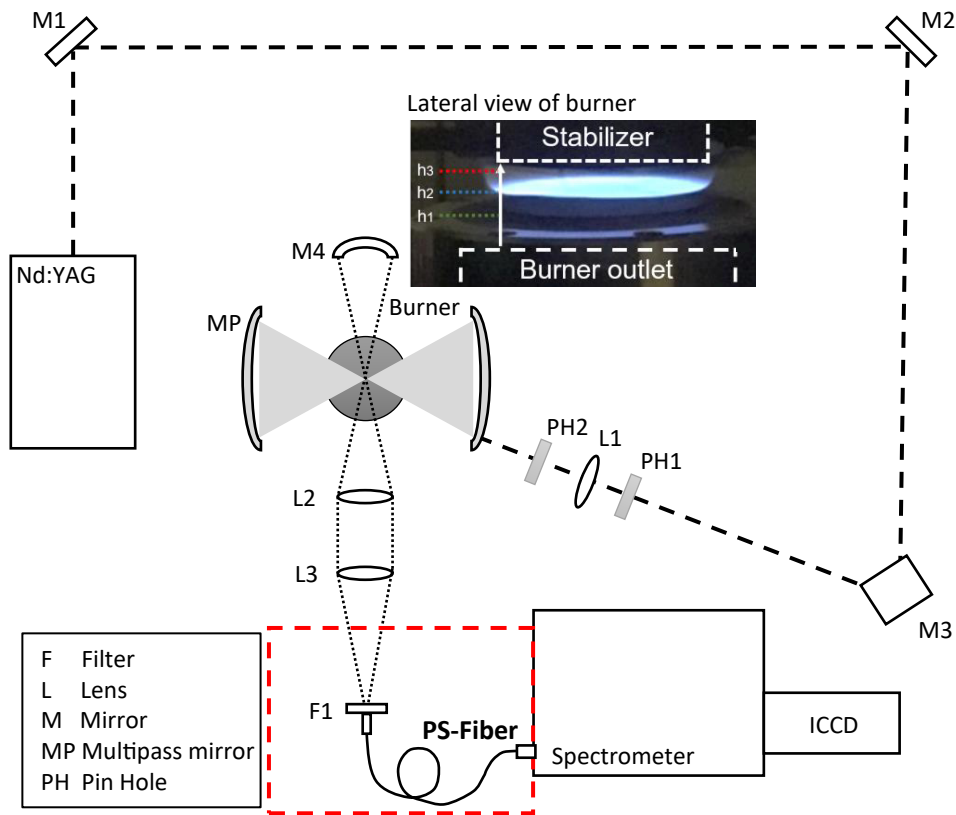


Fig. 5. Schematic of the experimental setup with a 532 nm laser beam employed to measure Raman scattering signals in a porous-plug burner. The burner can be adjusted in the vertical direction for measurements at different heights in the flame. The dashed red box marks out the insertion of the PS fiber in the setup.

of 150 mm was placed on the other side of the spectrometer to reflect signal scattered in this direction back towards the spectrometer, which theoretically increases the signal by a factor of 2. The collected Raman signal was focused onto the input end of the PS fiber, transmitted through the fiber bundle, and formed the PS modulation at the output end, placed at the entrance slit of the spectrometer. The transmitted signal was guided into the spectrometer (Princeton Instruments IsoPlane SCT 320) after a long-pass filter (F1, Semrock EdgeBasic BLP01-532R-25), which reduces light at the laser wavelength. The f -number of the collecting lenses, $f/4$, is selected to approximately match that of the spectrometer, $f/4.6$. However, this slight mismatch will cause a signal loss in the spectrometer since it is slightly overfilled. This corresponds to an NA value of 0.125, i.e., smaller than that of the PS-fiber, which is then underfilled by the light cone. Nevertheless, it was also noted that some imperfection in the manufacture of the PS-fiber prototype leads to some signal loss. For example, slight unevenness on the sizes and spacing of the individual fibers may lead to inaccurate numerical aperture.

The spectrometer was equipped with a grating of groove density 2400 lines/mm for measurements at high spectral resolution. An intensified CCD camera (Princeton Instruments PI-MAX4) was mounted at the output of the spectrometer. The on-CCD accumulation and intensifier gain parameters were set for optimal use of the dynamic range. The number of accumulations varied from 10000 to 300000 in order to achieve adequate photon counts for different measurement

conditions. All the spectra were corrected for a background measured with the laser beam blocked using equal detection settings.

A porous-plug flat-flame McKenna burner was placed at the probe volume in the multi-pass cell with the probe volume located above the burner surface. The burner was placed on a vertical translation stage in order to adjust the height of the probe volume above the burner. The burner was used both for generating room-temperature gas flows of air, nitrogen, and oxygen and for stabilizing a flame. Flame measurements were conducted in a stoichiometric premixed methane/air flame of equivalence ratio of 1.0 at heights above burner (HAB) of 3, 7, and 12 mm. The flame was lifted from the burner surface (cf. Figure 5) by adding an excessive nitrogen flow to the air, and the reaction zone was located approximately 7 mm above the burner surface. Measurements at the flame front are challenging using a multi-pass arrangement due to strong temperature gradients that cause beam steering. These measurements were acquired at stable flame conditions that, with the current measurement setup, minimized the problem of beam steering to slight adjustments of one of the multipass cavity mirrors. A metal plate for stabilizing the flame was placed 19 mm above the burner. The total gas flow rate was set to 22.32 NLPM, and the nitrogen/oxygen ratio was 6.69.

In order to quantitatively analyze the spectra, the software PGOPHER [34] was employed for modeling the theoretical spectra of nitrogen, oxygen, and carbon dioxide, using molecular constants from the literature [9, 35]. Temperature and oxygen mole fraction were evaluated by fitting theoretical spectra to the experimental spectra. The theoretical spectra were calculated for different compositions of $N_2/O_2/CO_2$ and temperature. The evaluated temperature and oxygen mole fraction were retrieved from the theoretical spectrum that gave the best fit of the experimental one.

3. Results and discussion

Raman spectra were recorded in wavenumber ranges $0-500\text{ cm}^{-1}$ and $2000-2500\text{ cm}^{-1}$ to study the effect of the fiber-based PS method. The low-wavenumber region ($0-500\text{ cm}^{-1}$) is where the pure rotational Raman S-branch lines are located, and this spectral range is significantly affected by the laser-induced stray light. Therefore, it is suitable to study the performance of the stray-light suppression process in this region. The region of $2000-2500\text{ cm}^{-1}$ is where the nitrogen ro-vibrational O-, Q-, and S-branches are located and is less affected by stray light.

3.1. Spectral analysis from room-temperature gas mixtures

Raman spectra in the wavenumber range $0-300\text{ cm}^{-1}$ and $2000-2500\text{ cm}^{-1}$ from room-temperature air, oxygen, and nitrogen were investigated. Data are compared before and after they have been processed with the lock-in-based periodic shadowing analysis. The intensity of each spectrum was normalized to the maximum of the after-PS spectrum for better visibility. As shown in Fig. 6, the fiber-based PS method is efficient for stray-light suppression, especially in the low-wavenumber region (a-b) where the pure rotational Raman peaks are located close to the laser line and therefore strongly affected by stray light. The increased level of stray light in this spectral region arises from multiple scattering and reflections of the incident laser light, which are significantly stronger than the Raman signal. The ratio between the signal intensity before and after the PS process is displayed under each spectrum, showing a large improvement in peak contrast where the stray-light interference level is reduced by a factor of up to 80 in the region $0-50\text{ cm}^{-1}$. The PS process also reveals the concealed temperature-dependent intensity distribution of the pure rotational S-branch lines, which indicates the possibility for quantitative temperature evaluation (which will be discussed in section 4.2). An increase of the stray light in the region $2000-2500\text{ cm}^{-1}$ is also caused by the superposition of wings from strong lines nearby [24], in this case, the nitrogen Q-branch at 2331 cm^{-1} (cf. Figure 6(c)). The smaller ro-vibrational S-branch peaks

adjacent to the strong Q-branch peak are revealed with a more accurate intensity distribution after PS processing.

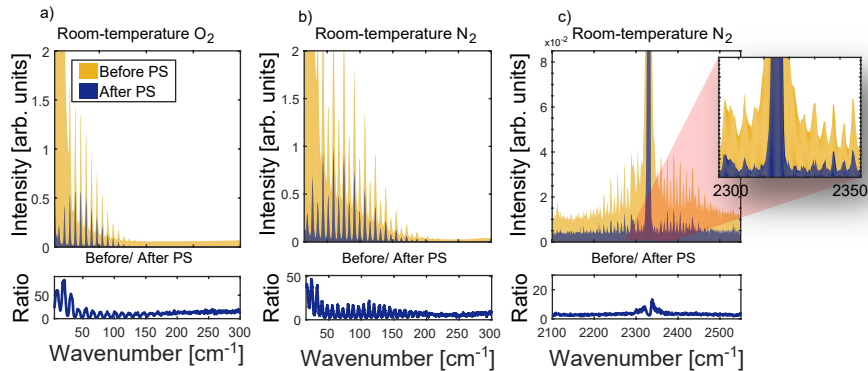


Fig. 6. Raman spectra from room-temperature oxygen and nitrogen at two spectral regions, before (yellow) and after (blue) the PS process. The ratio between the intensity before and after the PS process is plotted below each spectrum. a)-b) pure rotational S-branch spectra of oxygen and nitrogen. c) Q-branch ro-vibrational spectrum of nitrogen.

Figure 7 shows the pure rotational Raman S-branch spectrum of air at room temperature. Similar to the results of Fig. 6, stray light at lower wavenumber values is effectively removed in the PS processing. The spectrum retrieved after PS processing can be well fitted to a theoretical spectrum of temperature 300 K and an O₂ mole fraction of 21%, in agreement with the experimental conditions. This confirms the reliability of the fiber-PS method, as the fit reveals excellent agreement with a correlation value R^2 of 0.99.

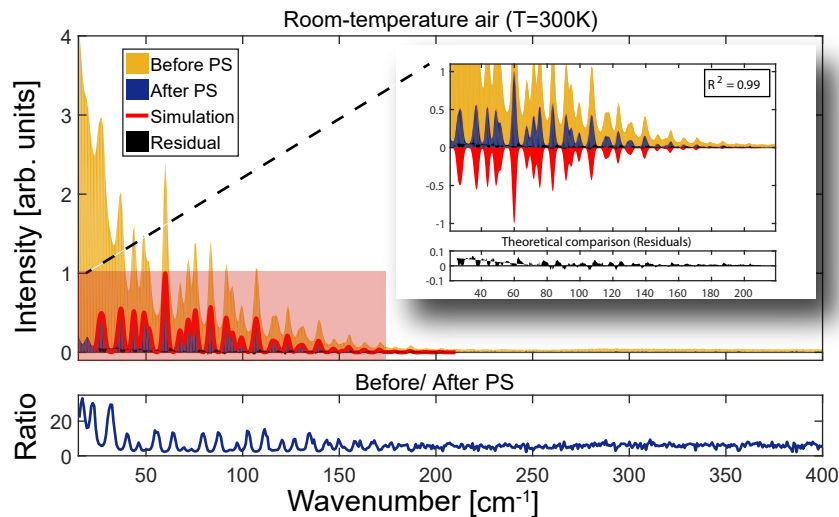


Fig. 7. Pure rotational Raman spectrum from room-temperature air. The theoretical spectrum of temperature 300 K (red) shows excellent agreement with the PS processed spectrum (blue), and the evaluated composition of air agrees well with the actual value (79% nitrogen and 21% oxygen).

3.2. Suppression of different stray-light levels

Different stray-light levels were achieved by placing a scattering object near the probe volume when rotational Raman spectra were acquired. Four sets of 100 spectral images consisting of 2500 on-chip accumulations each, corresponding to an acquisition time of 0.5 s, were recorded for each stray-light level. Averaged data with background levels subtracted are displayed in Fig. 8 for all four cases with different amounts of stray light (Level 1-4). The levels of stray light has a significant impact on the spectra up to about 50 cm^{-1} , where it drops to more moderate levels. Nevertheless, the spectrum that has been processed by periodic shadowing indicates that all levels of stray-light make a significant contribution to the spectrum up to at least 150 cm^{-1} compared to the Raman signal. Data were acquired in these sets in order to investigate the impact of the fiber-PS process on the accuracy and precision of temperature and O_2 mole fractions retrieved from the spectra. Due to severe stray-light interference levels, it was not possible to fit the spectra before the PS process at wavenumber values lower than 50 cm^{-1} . On the other hand, the spectra after PS process could be fitted from 20 cm^{-1} . Thus, the lower limits for fitting were set to 50 cm^{-1} and 20 cm^{-1} for the before- and after- fiber-PS process, respectively.

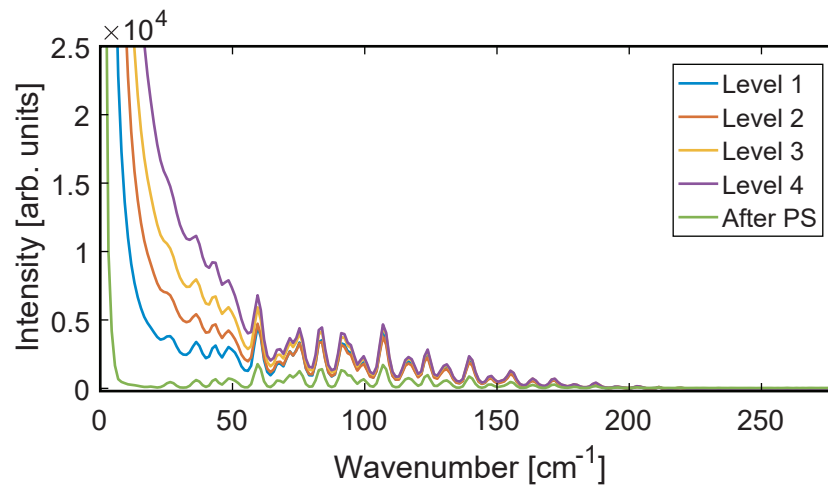


Fig. 8. Pure rotational S-branch Raman spectra measured with different amounts of stray light (Level 1-4). The green curve displays data (the Level 1 case) that has been processed using periodic shadowing where much of the stray light has been suppressed.

The evaluated average oxygen mole fractions and temperatures of each case together with corresponding standard deviations in parenthesis are listed in Table 2. The spectra contain a constant residual baseline that can be accounted for in the fit to evaluate temperature and mole fraction. For the lowest stray-light level, the unprocessed and PS-processed spectra give the same oxygen mole fraction, 20.7%, and the evaluated results then increase with stray-light level. For fiber-PS data, the increase is marginal, and all results are close to the expected value for air, 21%. For the unprocessed data, the increasing trend is stronger, and the values gradually deviate more from the correct value. The spectra were measured at $\sim 295\text{ K}$, and the evaluated temperatures of the PS-processed data are 3-14 K lower. The deviation from the expected temperature shows a slight increase with the stray-light level. However, the unprocessed data result in much lower temperatures that are not realistic for measurements at ambient conditions. This is most likely due to stray-light contribution at the lower wavenumber values of the spectrum, which biases the evaluation towards lower temperature.

Table 2. Evaluated oxygen mole fractions and temperatures with corresponding standard deviations. Expectation values for oxygen mole fraction and temperature is 21% and 295 K, respectively.

	Evaluated oxygen mole fraction (%)		Evaluated temperature (K)	
	Before fiber-PS	After fiber-PS	Before fiber-PS	After fiber-PS
level1	20.7	20.7 (1.4)	269	292 (11)
level2	21.4	20.8 (1.4)	227	287 (11)
level3	22.0	20.9 (1.4)	211	286 (8)
level4	23.7	21.1 (1.2)	-	281 (9)

The evaluated temperatures for raw data without periodic shadowing filtering show smaller standard deviations with increased stray-light background levels. This is due to the fact that the raw data is dominated by a rather stable stray-light contribution that does not vary considerably compared with the Raman peaks. Hence, standard deviations for raw data are not presented here to avoid confusion. The standard deviation in O₂ mole fraction and temperatures, evaluated from after fiber-PS data, display small variation for the four different stray-light levels. Thus, the fiber-PS process has a low impact on the accuracy as well as precision of data evaluated from the spectra.

3.3. Temperature measurements in premixed methane-air flame

Temperature evaluation was made for spectra measured at three different heights in a premixed stoichiometric methane/air flame, as shown in Fig. 9. The selected heights above burner (h1 = 3 mm, h2 = 7 mm, h3 = 12 mm) represent the reactant zone (low temperature), the preheat zone (medium temperature), and the post-flame zone (high temperature), respectively. The low-temperature (h1) case displays pure rotational lines of oxygen and nitrogen from the air. Further, the spectrum at medium temperature (h2) shows rotational lines from nitrogen, remaining oxygen, and carbon dioxide formed as a result of the combustion. As for the high-temperature (h3) case, where the oxygen is mostly consumed and carbon dioxide is fully formed, the spectrum mainly consists of nitrogen lines superimposed with carbon dioxide lines.

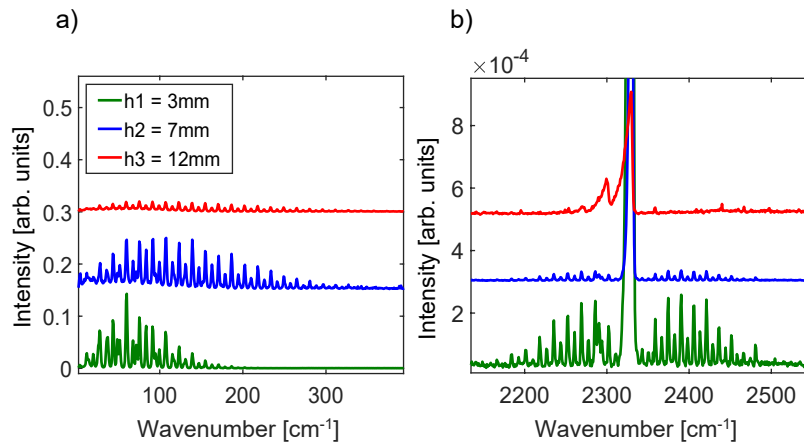


Fig. 9. After PS Raman spectra of a stoichiometric methane/air premixed flame at different heights (h1, h2, h3). a) pure rotational S-branch spectra; b) ro-vibrational Q-branch N₂ spectra. The intensity of each spectrum is normalized by unit acquisition time to illustrate the relative intensity.

The evaluation was performed by fitting experimental spectra with simulated spectra of multi-species (nitrogen, oxygen, and carbon dioxide) pure rotational lines and ro-vibrational nitrogen lines, respectively. For simulations of rotational spectra, the mole fraction of each species at the different heights was estimated in our earlier work [37] by inspection of spectra and calculation of product gas composition. The deduced vibrational temperature is typically higher than the rotational temperature, especially in the high-temperature region. This is caused by the difference in temperature sensitivity of the spectral features used for temperature evaluation in the two cases, the envelope of the pure nitrogen rotational S-branch lines and the Q-branch vibrational hot band. The envelope of the rotational lines becomes less sensitive at higher temperatures, which results in decreased sensitivity, bringing inaccuracy when comparing to the other approach using the vibrational hot band. The evaluated temperatures from the two wavenumber regions are listed in Table 3, where a good agreement between the two approaches is shown at the intermediate temperature where both types of spectra are sensitive, with deviations of the tabulated values around 5%. Temperature measurements can be made with high accuracy for methods based on Raman spectrum analysis, as demonstrated for Coherent Anti-Stokes Raman Spectroscopy (CARS), a well-characterized benchmark method for gas-phase thermometry in combustion diagnostics [6,9]. The CARS method has been employed for studies in flames of the same type as presented here, and temperature uncertainties on the order of a few percent have been reported [36, 38]. Thus, a similar temperature accuracy should be feasible for measurements with Raman spectroscopy as presented here, but calibration is required for the determination of the temperature uncertainty. The product zone temperature, 1519 K, obtained for the stoichiometric flame is rather low. However, the high nitrogen-to-oxygen ratio of the reactants used to obtain a flame lifted from the burner surface resulted in a diluted flame for which rather low temperatures can be expected.

Table 3. Evaluated temperatures at the different heights in the flame.

	Evaluated temperatures (K)	
	From the rotational Raman spectrum of air/nitrogen	From the vibrational Raman spectrum of nitrogen
h1	292	329
h2	985	1027
h3	1294	1519

The fitted temperatures from the evaluation of the nitrogen vibrational spectra were used as input for the simulations of pure rotational spectra to check the consistency between rotational and vibrational Raman measurements. The calculated rotational spectra show an excellent match with the experimental data, as shown in Fig. 10. Note that the intensity of the simulation in each case is normalized by the maximum of the measured spectrum after PS in order to compare. The excellent agreement between the experimental and theoretical spectra further confirms the feasibility and reliability of the fiber-based PS method. In addition, it needs to be noted that background varies in every measurement due to the uniqueness of each measuring condition. As a result of the spectral resolution of the system, individual carbon dioxide rotational lines cannot be resolved but are observed as a combined broad spectral feature at wavenumber value shifts up to $\sim 150 \text{ cm}^{-1}$. Nevertheless, the envelope of the pure rotational CO_2 S-branch lines is exposed after the stray light is removed using the fiber PS method. This envelope is, however, completely concealed by the stray light before the PS process is applied.

3.4. Noise reduction

Frequencies that are not associated with the signal modulation are removed when the band-pass filter is applied. Thus, a ‘cleaner’ spectrum is expected after the PS process with higher

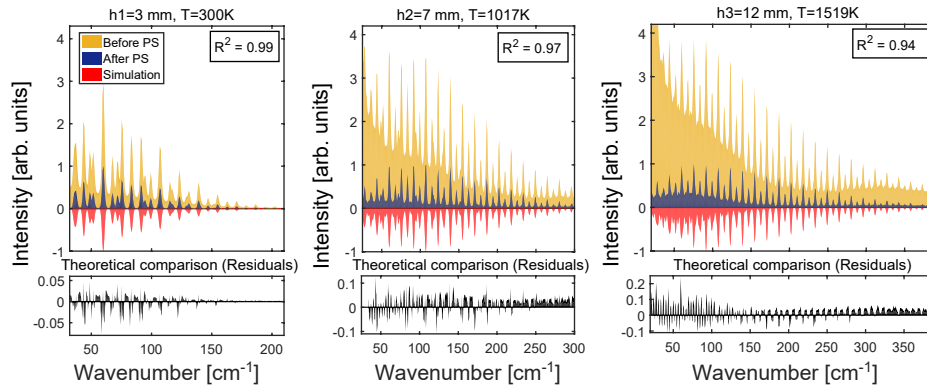


Fig. 10. Comparison between the pure rotational S-branch Raman spectra from three different positions in the methane flame before PS (yellow), after PS (blue), and the corresponding simulation (red). For clarity, the intensity of the simulations is plotted in the reverse direction.

signal-to-noise ratios. This was also confirmed in the previous study by Kristensson et al. [27], where the PS concept was implemented using a Ronchi grating. Figure 11 shows a statistical analysis of a rotational Raman spectral image measured in room-temperature air. The histograms show the intensity distributions of the image measured in room-temperature air. The histograms show the intensity distributions of the image measured in room-temperature air. The histograms show the intensity distributions of the image measured in room-temperature air. The histograms show the intensity distributions of the image measured in room-temperature air. A comparison shows that the standard deviation σ , representing the noise level, is reduced by a factor of 4, and the signal-to-noise ratio is then estimated to improve by at least a factor of 2. These results indicate that the implementation of periodic shadowing is beneficial in fiber-based spectroscopy since the technique itself increases the signal-to-noise ratio by the mode-locking-based signal processing. In addition, more light can be collected by the fiber bundle, which also is beneficial from a signal-to-noise point of view. Using a fiber bundle instead of a single fiber does, however, cause a loss in spatial resolution, but the current fiber-bundle input configuration, shown in Table 1 and Fig. 4, displays effective use of the fiber-input area. The presented technique would not give much benefit in measurement situations with strong signals, well-separated spectral features, effective optical filters, and limited stray light interferences, but otherwise, the combination of effective light-collection abilities and suppression of scattered light makes it ideal for Raman spectroscopy.

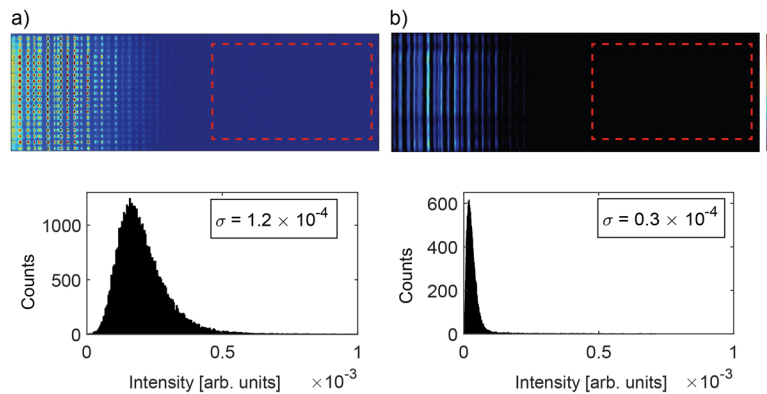


Fig. 11. Improvement of noise level after PS process of a fiber-PS rotational Raman spectrum in room-temperature air. The histograms show the pixel intensity distribution for the image region indicated by the red rectangle and a reduction of the noise level by a factor of 4.

4. Conclusion

In summary, a fiber-based stray-light suppression method for spectroscopic measurements has been presented and demonstrated in Raman spectroscopy of gases. The principle of the method is the implementation of a specialized fiber to perform the Periodic Shadowing method, where the signal light is guided and modulated into a predefined pattern before entering the spectrometer. With further processing algorithms based on spatial lock-in amplification, the stray light can be correctly and efficiently suppressed, in this study by up to a factor of 80. Analysis of Raman spectra showed that correct quantitative information on species mole fractions and temperature could be retrieved from processed data. In addition to the stray-light suppression ability, the fiber-based PS method brings improved flexibility to the detection system. These features together make the concept highly valuable for accurate spectroscopic measurements in experiments with limited optical access.

Funding. Stiftelsen för Strategisk Forskning (ITM17-0313); Energimyndigheten (22538-4); Knut och Alice Wallenbergs Stiftelse (2019.0084); European Research Council (669466, 803634, 852394); Vetenskapsrådet (2015-04056, 2015-05321).

Disclosures. The authors declare no conflicts of interest.

References

1. W. Demtröder, *Laser spectroscopy*. Vol. 2, Springer (1973).
2. C. N. Banwell and E. M. McCash, "Fundamentals of molecular spectroscopy," Vol. 851.: McGraw-Hill New York (1994).
3. A. Downes and A. Elfick, "Raman spectroscopy and related techniques in biomedicine," *Sensors* **10**(3), 1871–1889 (2010).
4. M. Baudelet, "Laser spectroscopy for sensing: fundamentals, techniques and applications," / edited by Matthieu Baudelet. Woodhead publishing series in electronic and optical materials, Amsterdam: Woodhead Publishing. xxiv, 565 pages, 8 unnumbered pages of plates (2014).
5. V. P. Gupta, "Molecular and laser spectroscopy: advances and applications," Elsevier, Amsterdam, Netherlands. xvi, 346 pages (2018).
6. K. Kohse-Höinghaus and J.B. Jeffries, eds. "Applied Combustion Diagnostics," Taylor&Francis: New York (2002).
7. R. Ono, "Optical diagnostics of reactive species in atmospheric-pressure nonthermal plasma," *J. Phys. D: Appl. Phys.* **49**(8), 083001 (2016).
8. S. D. Schwab and R. L. McCreery, "Versatile, efficient Raman sampling with fiber optics," *Anal. Chem.* **56**(12), 2199–2204 (1984).
9. A. C. Eckbreth, "Laser diagnostics for combustion temperature and species," Vol. 3, CRC press. (1996).
10. R. Donaldson, "Stray light in monochromators," *J. Sci. Instrum.* **29**(5), 150–153 (1952).

11. J. K. Pribram and C. M. Penchina, "Stray light in Czerny-Turner and Ebert spectrometers," *Appl. Opt.* **7**(10), 2005–2014 (1968).
12. E. C. Fest, "*Stray Light Analysis and Control*", SPIE Press (2013).
13. A. W. S. Tarrant, "Optical Techniques for Studying Stray Light in Spectrophotometers," *Opt. Acta* **25**(12), 1167–1174 (1978).
14. A. Bohlin and P. E. Bengtsson, "Effective Suppression of Stray Light in Rotational Coherent Anti-Stokes Raman Spectroscopy Using an Angle-Tuned Short-Wave-Pass Filter," *Appl. Spectrosc.* **64**(8), 964–966 (2010).
15. Z. S. Li, M. Afzelius, J. Zetterberg, and M. Aldén, "Applications of a single-longitudinal-mode alexandrite laser for diagnostics of parameters of combustion interest," *Rev. Sci. Instrum.* **75**(10), 3208–3215 (2004).
16. J. Bood, P. E. Bengtsson, and M. Aldén, "Stray light rejection in rotational coherent anti-Stokes Raman spectroscopy by use of a sodium-seeded flame," *Appl. Opt.* **37**(36), 8392–8396 (1998).
17. J. Bood, P. E. Bengtsson, and T. Dreier, "Rotational coherent anti-Stokes Raman spectroscopy (CARS) in nitrogen at high pressures (0.1–44 MPa): experimental and modelling results," *J. Raman Spectrosc.* **31**(8–9), 703–710 (2000).
18. A. P. Yalin and R. B. Miles, "Temperature Measurements by Ultraviolet Filtered Rayleigh Scattering Using a Mercury Filter," *J. Thermophys. Heat Transfer* **14**(2), 210–215 (2000).
19. R. Claps, M. Fink, P. Varghese, and D. Young, "Thermodynamic Studies in Subsonic Gas Flows Using a Laser Diode Raman Spectrometer," *Appl. Spectrosc.* **54**(9), 1391–1398 (2000).
20. R. G. Seasholtz and A. E. Buggele, "Improvement in suppression of pulsed Nd:YAG laser light with iodine absorption cells for filtered Rayleigh scattering measurements," *Proc. SPIE* **3172**, 625–635 (1997).
21. R. B. Miles, L. Qian, and S. H. Zaidi, "Imaging flow structure and species with atomic and molecular filters," *Opt. Lasers Eng.* **44**(3–4), 240–260 (2006).
22. D. Landon and S. Porto, "A tandem spectrometer to detect laser-excited Raman radiation," *Appl. Opt.* **4**(6), 762–763 (1965).
23. A. Walsh, "Multiple Monochromators. II. Application of a Double Monochromator to Infrared Spectroscopy," *J. Opt. Soc. Am.* **42**(2), 96–100 (1952).
24. V. A. Fassel, J. M. Katzenberger, and R. K. Winge, "Effectiveness of interference filters for reduction of stray light effects in atomic emission spectrometry," *Appl. Spectrosc.* **33**(1), 1–5 (1979).
25. W. F. Maddams and M. J. Southon, "III. The effect of band width and band shape on resolution enhancement by derivative spectroscopy," *Spectrochim. Acta* **38**(4), 459–466 (1982).
26. D. G. Cameron and D. J. Moffatt, "A Generalized Approach to Derivative Spectroscopy," *Appl. Spectrosc.* **41**(4), 539–544 (1987).
27. E. Kristensson, J. Bood, M. Aldén, E. Nordström, J. Zhu, S. Hult, P. E. Bengtsson, H. Nilsson, E. Berrocal, and A. Ehn, "Stray light suppression in spectroscopy using periodic shadowing," *Opt. Express* **22**(7), 7711–7721 (2014).
28. M. A. Neil, R. Juškaitis, and T. Wilson, "Method of obtaining optical sectioning by using structured light in a conventional microscope," *Opt. Lett.* **22**(24), 1905–1907 (1997).
29. J. H. Scofield, "Frequency-domain description of a lock-in amplifier," *Am. J. Phys.* **62**(2), 129–133 (1994).
30. E. Smith and G. Dent, "Modern Raman spectroscopy: a practical approach," John Wiley & Sons (2019).
31. K. C. Utsav, J. A. Silver, D. C. Hovde, and P. L. Varghese, "Improved multiple-pass Raman spectrometer," *Appl. Opt.* **50**(24), 4805–4816 (2011).
32. G. Magnotti, K. C. Utsav, P. L. Varghese, and R. S. Barlow, "Raman spectra of methane, ethylene, ethane, dimethyl ether, formaldehyde and propane for combustion applications," *J. Quant. Spectrosc. Radiat. Transfer* **163**, 80–101 (2015).
33. A. Ehn, J. J. Zhu, X. Li, and J. Kiefer, "Advanced laser-based techniques for gas-phase diagnostics in combustion and aerospace engineering," *Appl. Spectrosc.* **71**(3), 341–366 (2017).
34. C. M. Western, "PGOPHER: A program for simulating rotational, vibrational and electronic spectra," *J. Quant. Spectrosc. Radiat. Transfer* **186**, 221–242 (2017).
35. D. Spelsberg and W. Meyer, "Static dipole polarizabilities of N₂, O₂, F₂, and H₂O," *J. Chem. Phys.* **101**(2), 1282–1288 (1994).
36. A. Bohlin, A. Kindeya, E. Nordström, and P.-E. Bengtsson, "Validation of a rotational coherent anti-Stokes Raman scattering model for N₂O at temperatures from 295 K to 796K," *J. Raman Spectrosc.* **43**(5), 604–610 (2012).
37. M. Gong, "Development of Spectroscopic Measurements for Raman and Thomson Scattering Diagnostics - Applications in Combustion and Plasma," M.S. thesis (Department of Physics, Lund University, 2019).
38. L. Martinsson, P.-E. Bengtsson, M. Aldén, S. Kröll, and J. Bonamy, "A test of different rotational Raman linewidth models: Accuracy of rotational coherent anti-Stokes Raman scattering thermometry in nitrogen from 295 to 1850K," *J. Chem. Phys.* **99**(4), 2466–2477 (1993).